DuRoss, C.B., et al., 2022, Portable optically stimulated luminescence age map of a paleoseismic exposure: Geology, https://doi.org/10.1130/G49472.1

Electronic Supplement

Portable optically stimulated luminescence age map of a paleoseismic exposure

Christopher B. DuRoss[1], Ryan D. Gold[1], Harrison J. Gray[2], and Sylvia Nicovich[3]

[1] U.S. Geological Survey, Golden CO
[2] U.S. Geological Survey, Denver CO
[3] Bureau of Reclamation, Denver CO

Deep Creek Site

At the Deep Creek site in central Utah (39.507462°, -111.861790°), the Wasatch fault zone is expressed as a 3-m-high normal fault scarp that crosses a Holocene alluvial fan surface. Incision along Deep Creek has exposed alluvial fan gravel and evidence of a single earthquake surface rupture.

We occupied the Deep Creek site in 2019–2020, cleaned the exposure back ~20–50 cm using hand tools, mapped the stratigraphy, structure, and pedogenic horizons on photomosaics (after Reitman et al., 2015) for a ~3-m-long portion of the exposure, and sampled for geochronology (Figure S1). Descriptions of stratigraphic units exposed at the site can be found in Jackson (1991) and Hylland and Machette (2008).

Geochronological Methods

We extracted 35 bulk-sediment samples of the alluvial fan, paleosol, and scarp-derived colluvial wedge exposed at the Deep Creek site. The sample areas were rectangular with long axes oriented parallel to bedding and ranged from 60–300 cm^2, with one large (500 cm^2) sample in the alluvial fan sediment. In the paleosol, four groups of 2–3 vertically stacked samples span nearly the entire thickness of the soil. Sample processing and charcoal extraction from the bulk samples were conducted by PaleoResearch Institute (Golden, Colorado). Charcoal from the bulk soil samples yielded 23 radiocarbon (^{14}C) ages (excluding three modern ages; Table S1), which we calendar calibrated using OxCal (Bronk Ramsey, 2009) and the IntCal20 terrestrial calibration curve (Reimer et al., 2020).

Eleven single-aliquot optically stimulated luminescence (OSL) samples consisted of bulk sediment collected from the alluvial fan, paleosol, and scarp colluvium using dark-room conditions (e.g., Gray et al., 2015; Tables S2, S3). Rectangular sample areas were oriented parallel to bedding and ranged from 80 to 150 cm^2. The OSL of fine (90-250 µm) quartz sand was measured to produce 11 OSL ages (Table S3), which we modeled using minimum and central age models (Galbraith and Roberts, 2012). Sediment from near the sample areas was evaluated for background radiation (laboratory measured dose rate), and sediment augured from the colluvial-wedge surface to a depth of ~1 m as well as ~1 m horizontally into the footwall alluvial fan exposure yielded sediment saturation estimates.

Radiocarbon and OSL ages for the Deep Creek site are shown in Tables 1–3 and included in Gray et al. (2021).

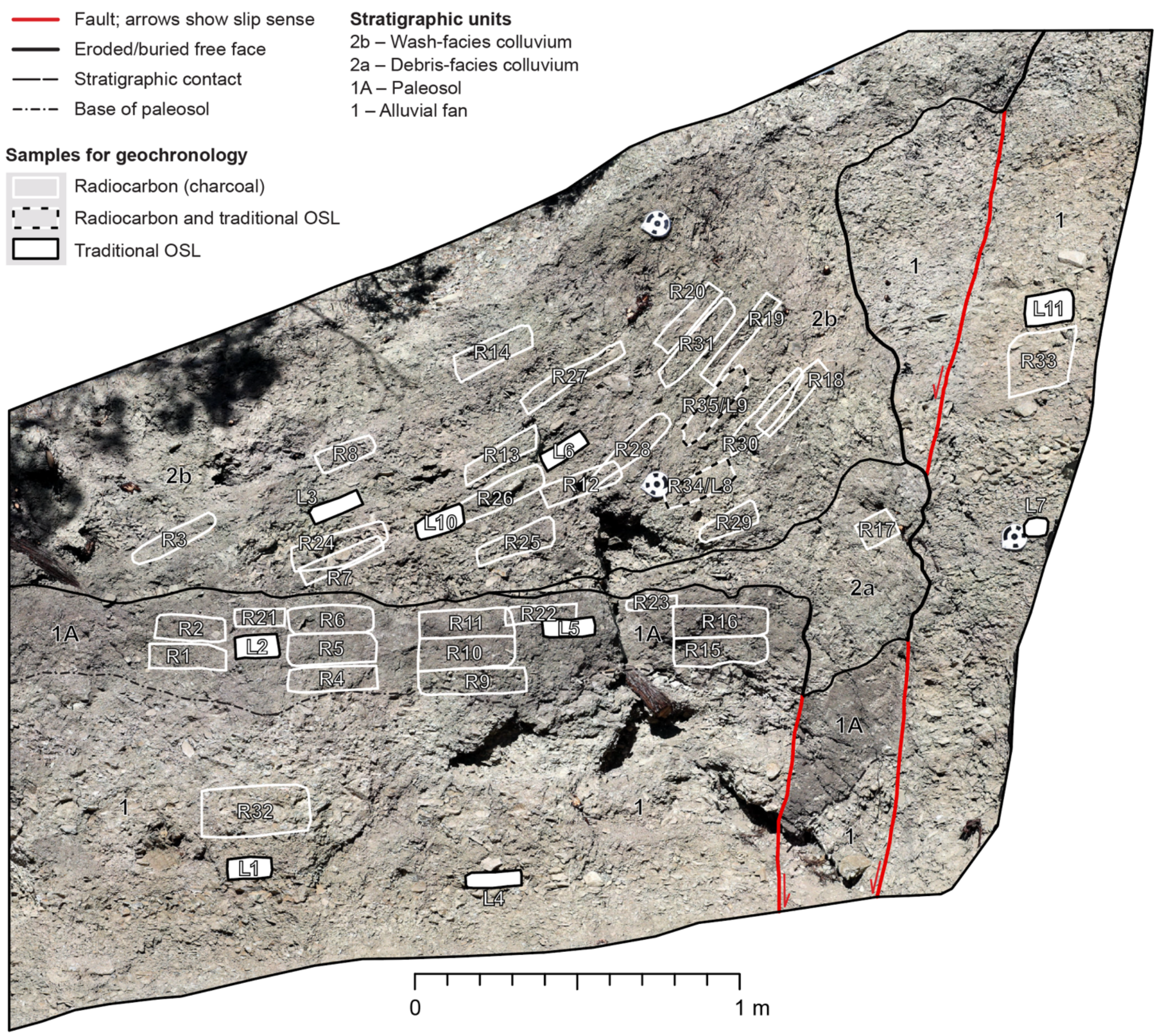

Figure S1. Bulk sediment samples of the Deep Creek paleoseismic exposure for ^{14}C and optically stimulated luminescence (OSL) dating. Sample numbers correspond to Tables S1–S3. Basemap is photomosaic generated using the methods of Reitman et al. (2015).

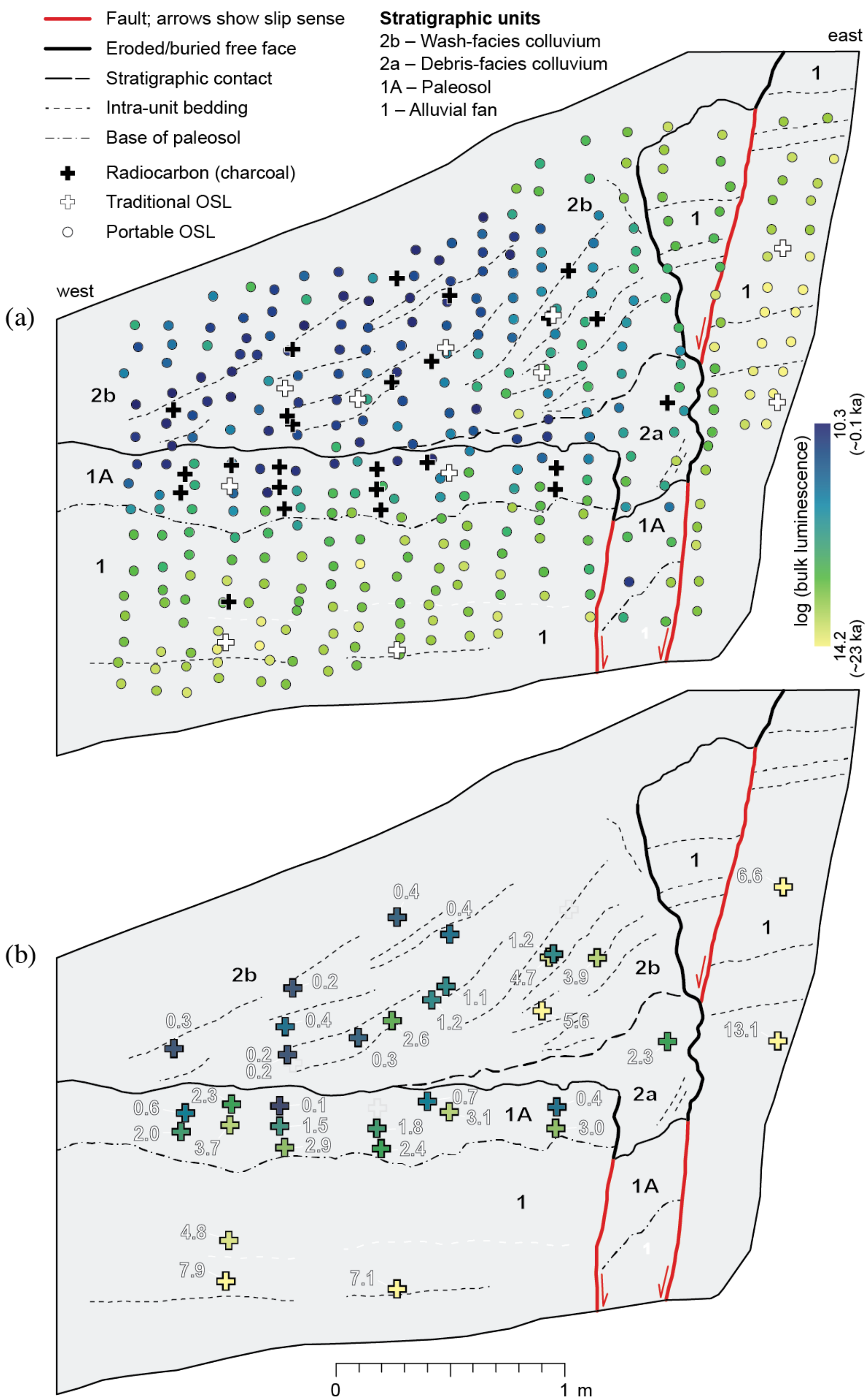

Figure S2. a) [14]C, OSL, and portable OSL samples span the Deep Creek paleoseismic exposure, and b) yield geochronological constraints on alluvial fan (unit 1) deposition, paleosol (unit 1A) formation, and scarp-derived colluvial (units 2a and 2b) sedimentation.

Table S1. Radiocarbon Ages for the Deep Creek Site

Sample Number[1]	Sample Description[2]	Lab Age (^{14}C yr B.P.)[3]	D^{13}C[4]	Calibrated Age (cal yr B.P.)[5]	Accession Number[6]
DC-R1	Conifer, UID (0.7)	2030 ± 20	-	1970 ± 30	OS-156084
DC-R2	UID (1.5)	540 ± 20	-	550 ± 30	OS-156085
DC-R3	UID (8.8)	245 ± 15	-	270 ± 60	OS-156296
DC-R4	Conifer (1.6)	2820 ± 20	-	2920 ± 30	OS-156087
DC-R5	Conifer, UID (0.5)	1600 ± 25	-	1470 ± 40	OS-156088
DC-R6	UID (0.6)	130 ± 20	-	130 ± 80	OS-156123
DC-R7	UID (0.5)	>modern	-	-	OS-156124
DC-R8	Conifer, UID (2.4)	225 ± 15	-	230 ± 70	OS-156089
DC-R9	Conifer (0.8)	2370 ± 20	-	2380 ± 40	OS-156125
DC-R10	UID (1.1)	1880 ± 20	-	1780 ± 30	OS-156116
DC-R11	UID (0.8)	>modern	-	-	OS-156126
DC-R12+R13	UID (0.8)	1310 ± 20	-	1230 ± 40	OS-156127
DC-R14	UID (4.0)	280 ± 15	-	350 ± 50	OS-156090
DC-R15	UID (1.1)	2890 ± 20	-	3020 ± 40	OS-156117
DC-R16	UID (0.4)	355 ± 25	-	400 ± 50	OS-156128
DC-R17	UID (0.4)	2270 ± 40	-	2250 ± 60	OS-156193
DC-R19	UID (0.9)	>modern	-	-	OS-156129
DC-R21	UID (1.4)	2310 ± 20	-23.3	2330 ± 30	OS-160006
DC-R22	UID (0.5)	730 ± 20	-	670 ± 10	OS-160007
DC-R24a	UID (6.2)	175 ± 20	-28.4	170 ± 90	OS-160082
DC-R24b	UID (3.5)	220 ± 15	-25.1	220 ± 70	OS-160083
DC-R26	UID twigs (0.9)	2500 ± 25	-	2600 ± 70	OS-160008
DC-R27	UID twigs (3.5)	315 ± 55	-23.2	380 ± 70	OS-160116
DC-R32	Conifer (2.6)	4230 ± 20	-24.4	4800 ± 50	OS-160084
DC-R35	UID (1.0)	4130 ± 35	-24.1	4680 ± 90	OS-160009
DC-R18+R30	UID (0.5)	3560 ± 55	-	3850 ± 90	OS-160010

[1]Charcoal samples from the Deep Creek exposure (Figure S1); + indicates combined samples.
[2]Charcoal separation and identification by PaleoResearch Institute (Golden, Colorado); UID – unidentified charcoal. Total weight of sample in milligrams included in parentheses.
[3]Laboratory-reported radiocarbon age and 1σ error in ^{14}C yr B.P. (before present, 1950 CE).
[4]Delta ^{13}C, if measured.
[5]Calibrated age is mean ± 1σ; ages and errors rounded to nearest decade. Calendar calibrated using OxCal (v.4; Bronk Ramsey, 2009).
[6]Samples processed by the National Ocean Sciences Accelerator Mass Spectrometry Facility, Woods Hole Oceanographic Institution (Woods Hole, Massachusetts).

Table S2. Dose Rate for Deep Creek Optically Stimulated Luminescence Samples

Sample No.[1]	Water content[2]	K^3 (%)	U^3 (%)	Th^3 (%)	D_R[4] (Gray/ka)	N[5]	Over-dispersion[6]
DC-L1	1 (28) [3]	1.0 ± 0.02	1.4 ± 0.04	4.1 ± 0.2	1.6 ± 0.04	20 (30)	43%
DC-L2	1 (36) [3]	1.3 ± 0.03	1.6 ± 0.05	5.3 ± 0.3	2.0 ± 0.05	17 (30)	41%
DC-L3	0 (22) [3]	1.4 ± 0.03	1.8 ± 0.05	6.1 ± 0.3	2.1 ± 0.05	9 (30)	64%
DC-L4	4 (24) [3]	1.3 ± 0.03	1.7 ± 0.05	5.2 ± 0.3	2.0 ± 0.05	20 (30)	34%
DC-L5	1 (39) [3]	1.4 ± 0.03	1.7 ± 0.05	5.3 ± 0.3	2.1 ± 0.05	15 (30)	52%
DC-L6	0 (29) [3]	1.3 ± 0.03	1.6 ± 0.05	4.9 ± 0.2	1.9 ± 0.05	10 (30)	62%
DC-L7	1 (25) [3]	1.5 ± 0.03	1.7 ± 0.04	6.1 ± 0.3	2.2 ± 0.05	19 (30)	25%
DC-L8	0 (21) [3]	1.4 ± 0.03	1.3 ± 0.04	4.3 ± 0.2	2.0 ± 0.05	14 (30)	27%
DC-L9	0 (34) [3]	1.4 ± 0.03	1.3 ± 0.04	4.5 ± 0.2	2.0 ± 0.05	13 (30)	61%
DC-L10	0 (31) [3]	1.5 ± 0.03	1.3 ± 0.04	4.7 ± 0.2	2.1 ± 0.05	9 (30)	54%
DC-L11	0 (21) [3]	1.5 ± 0.03	1.5 ± 0.04	5.0 ± 0.3	2.1 ± 0.05	21 (30)	23%

[1] Samples for single-aliquot quartz OSL dating from the Deep Creek exposure (Figure S1).
[2] Percent water content of field sample with saturated water content in parentheses; square brackets show the water content used in age calculation.
[3] K, U, and Th determined by high resolution Ge gamma spectroscopy or inductively coupled plasma mass spectrometry.
[4] Environmental dose rate (D_R) from bulk sediment collected at sample sites.
[5] Number of aliquots meeting acceptance criteria; total number of aliquots measured in parentheses.
[6] Statistical dispersion beyond that expected for a perfectly bleached sample.

Table S3. Optically Stimulated Luminescence Ages for the Deep Creek Site

Sample No.[1]	CAM D_e[2] (Gray)	CAM age[2] (ka)	MAM D_e[3] (Gray)	MAM age[3] (ka)
DC-L1	25.5 ± 2.5	16.2 ± 1.6	12.5 ± 1.4	7.9 ± 0.9
DC-L2	13.8 ± 1.4	6.9 ± 0.7	7.4 ± 0.8	3.7 ± 0.4
DC-L3	2.0 ± 0.4	0.9 ± 0.2	0.8 ± 0.1	0.4 ± 0.1
DC-L4	23.9 ± 1.8	12.1 ± 1.0	14.0 ± 1.6	7.1 ± 0.8
DC-L5	9.0 ± 1.2	4.4 ± 0.6	6.5 ± 0.5	3.1 ± 0.2
DC-L6	4.1 ± 0.8	2.1 ± 0.4	2.1 ± 0.3	1.1 ± 0.2
DC-L7	39.1 ± 2.2	17.8 ± 1.1	28.8 ± 2.3	13.1 ± 1.1
DC-L8	16.0 ± 1.2	8.2 ± 0.6	11.0 ± 1.2	5.6 ± 0.6
DC-L9	6.7 ± 1.1	3.4 ± 0.6	2.4 ± 0.5	1.2 ± 0.2
DC-L10	1.0 ± 0.2	0.5 ± 0.1	0.6 ± 0.2	0.3 ± 0.1
DC-L11	18.2 ± 0.9	8.7 ± 0.5	13.6 ± 1.1	6.6 ± 0.6

[1] Samples for single-aliquot quartz OSL dating from the Deep Creek exposure (Figure S1).
[2] Central age model (CAM) equivalent dose (D_e) and mean age. 2σ uncertainties reported.
[3] Minimum age model (MAM) D_e and mean age. 2σ uncertainties reported.

Portable OSL Measurement

We used portable OSL (Sanderson & Murphy, 2010) and the methods of Gray et al. (2018) to measure bulk luminescence across the exposure. We collected 342 portable OSL samples using dark room conditions over the 3-m-wide exposure in ~19 mostly vertical columns spaced ~15 cm horizontally and spanning 130–215 cm of the exposure vertically (Figure 3). Within the

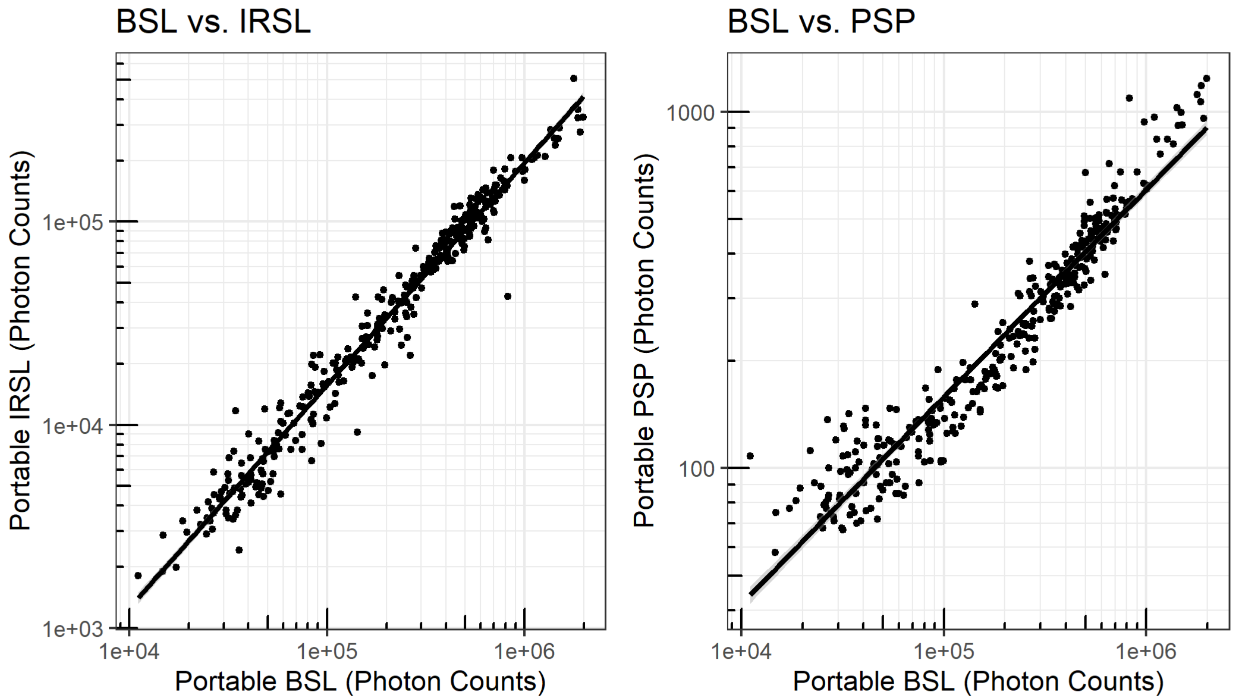

Figure S3: Plots of the weight-normalized blue-light stimulated luminescence (BSL) versus the infrared stimulated luminescence (IRSL) and the post stimulation phosphorescence (PSP). The use of either BSL, IRSL, or PSP measurements produces the same results. We use BSL in this study for simplicity.

columns, the portable OSL samples were vertically spaced 10–15 cm. Each sample consists of a small circular excavation area about 3–4 cm in diameter. The samples were collected without regard to stratigraphic contacts, faults, pedogenic horizons, or lateral changes in unit texture.

We processed the portable OSL samples in the laboratory by sieving each sample to the 90–250 µm grain size and separating aliquots weighing 0.5 ± 0.05 g. This aliquot weight results in a monolayer of grains at the base of the standard 50 mm single vent petri dishes (Model: 1200F46 Thomas Scientific) that are used in the portable OSL measurement. We measured the portable luminescence as photon counts using a SUERC Portable OSL Reader (acquired January 2017) (Sanderson and Murphy, 2010) with a protocol consisting of a 15-second dark count, 60-second measurement using IR LEDs, 30-second dark count, 60-second measurement with blue LEDs, and a final 30-second dark count. The portable OSL data were analyzed using the *Luminescence* package for the programming language R (Kreutzer et al., 2012; 2020 version). We found no difference in the results with either a 10- or 60-second integration interval, so we chose to integrate the total photon counts over the full 60-second measurement interval. The total photon counts are normalized by the sample weight to account for possible differences in photon counts due to varying numbers of grains (Gray et al., 2018). Because of some samples being extremely bright due to highly sensitive grains and to better show the 2D spatial relationships, we plot the logarithm of the weight normalized photon counts in Figure S2 and in figures in the main text.

We did not observe any significant differences in spatial patterns (and thus our results) between the blue-light stimulated luminescence (BSL) versus the infrared stimulated luminescence

(IRSL) measurements. Figure S2 shows a linear relationship between BSL and IRSL as well as a linear relationship between BSL and the post-stimulation phosphorescence (PSP). We solely used the BSL for the age regression for simplicity. The linear relation between BSL and IRSL suggests a nearly constant lithology of our portable OSL samples.

Portable OSL measurements for the Deep Creek site are included in Gray et al. (2021).

Portable OSL Bleaching Experiment

To test if the portable OSL measurement can be bleached (capable of being reduced or fully removed by sunlight exposure) and thus useful for age estimates, we conducted sunlight exposure experiments (Figure S3). We selected sample F.5-1 from the dataset and extracted 0.25 ± 0.005 g aliquots using the pretreatment procedures used in the main dataset. These aliquots were held in 50 mm single vent petri dishes (Model: 1200F46 Thomas Scientific) and exposed to sunlight for intervals of 0, 10, 30, 100, 300, 1000, 3000, and 10000 seconds (± 0.5 seconds) on 8 August 2020 starting at 10 am Mountain Daylight Time (MDT) at the patio of the southeastern door of Building 95 at the Denver Federal Center (39.7157, -105.1262). During each exposure interval, we recorded the average intensity of sunlight using an EXTECH Color LED Light Meter Model LT45 set to daylight mode, along with the start and stop times. After exposure, we measured these aliquots using the protocol described for the main dataset. The results of the experiment are plotted in Figure S1. We also performed two more rounds of bleaching experiment to evaluate any variance in the bleaching rate parameters. We used sample J-5 and B-2 to collect sediment from other parts of the parent material. J-5 was performed on 29 January 2021 starting at 11am Mountain Standard Time (MST) and finishing at approximately 2 pm MST, with mostly sunny skies. During part of the J-5 experiment, a diffuse cirrus-type cloud developed in front of the sun and decreased the lux by about 10-20 thousand for about 30 mins. The B-2 experiment was performed on 31 January 2021 under clear skies without clouds.

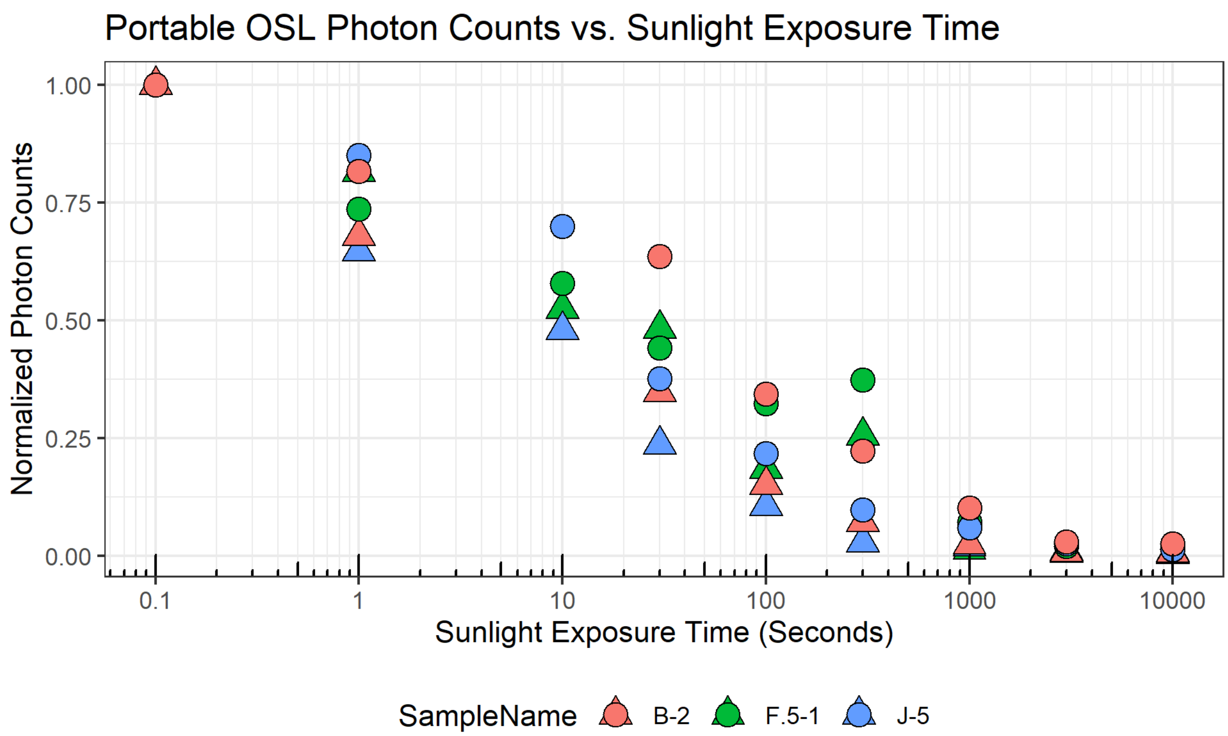

Figure S4: Plot of the results of the sunlight exposure experiment for three selected portable OSL samples. Aliquots of each sample were exposed to direct sunlight for varying time intervals and measured following the portable OSL measurement protocol. Circles show the BSL measurement and triangles show the IRSL measurement. All samples were reduced from the initial value to ~10% or less within 1000 seconds (~15 mins) and further reduced to less than 3% after 3000 seconds (~1 hour). Graph plotted with the ggplot2 package in the programming language R.

Portable OSL Age Calibration

For the age calibration, we collected subsamples from each full OSL age sample and measured these with the protocol described above. For ^{14}C samples, we used the interpolated portable OSL value as described below. Consistent with Stone et al. (2015), we found that a linear regression, between age and portable OSL best explained our data (Figure S4). We forced the regression through the origin as a free regression produces an equation with a y-intercept. Other researchers have found a linear regression between age and portable OSL produces a positive y-intercept value (Stone et al., 2015, 2019). However, we note that 'zero age' aliquots from our bleaching experiments still produce a small but measurable portable OSL. This zero age measurement is likely due to either slight age overestimations in the OSL and ^{14}C ages, a dark count photomultiplier tube artifact, or regenerating or very hard-to-bleach or unbleachable traps as sometimes observed in luminescence dating. Theoretically, the regression should produce a negative y-intercept and a positive x-intercept due to this zero age value. We decided to force the linear regression through the origin to reconcile the results of the bleaching experiment while noting that either a forced or unforced regression produces statistical overlap at the 95% confidence interval.

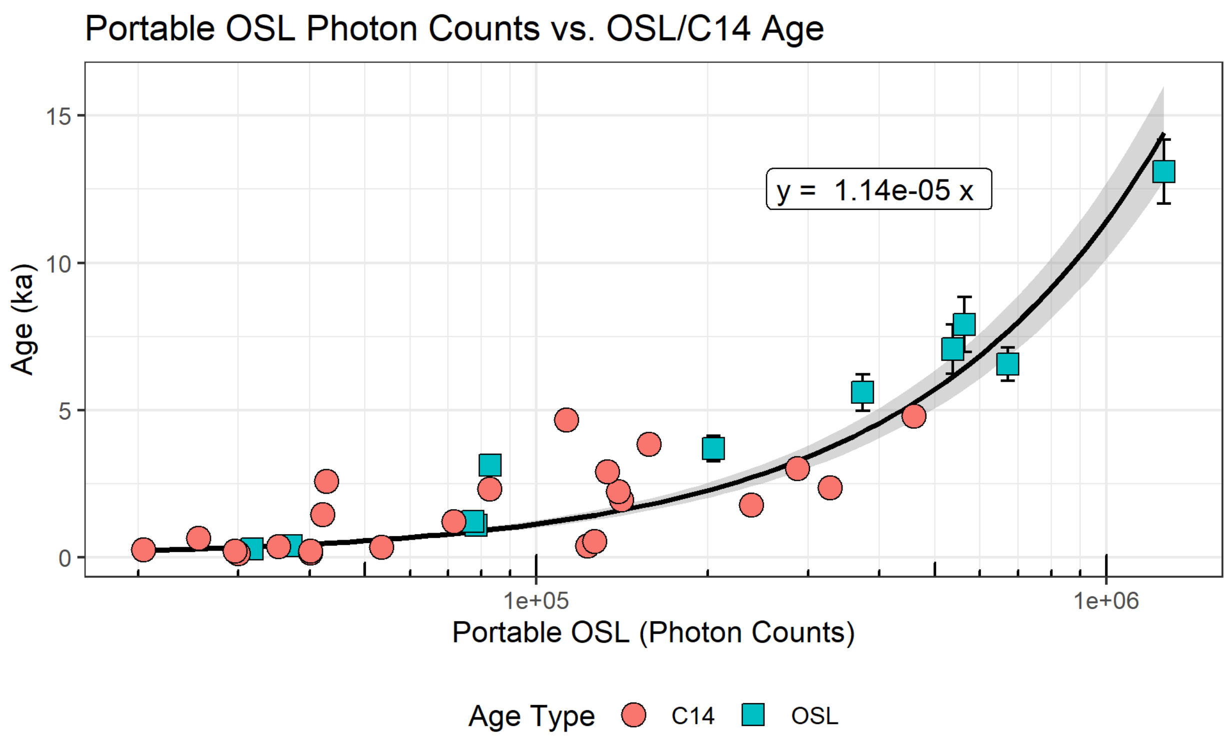

Figure S5: Linear regression between the weight-normalized portable OSL measurements (photon counts) and the ^{14}C and OSL ages. The statistically significant regression (adjusted R^2 = 0.91; p-value <2.12 × 10-16 at 95%) is shown with age on the y-axis because we use portable OSL measurement as the predictor variable in the age map (Figure 2B). The regression was performed using the lm() function and plotted with the ggplot2 package in the programming language R.

Portable OSL Surface Interpolation

We interpolated a portable OSL bulk-luminescence surface using the portable OSL point data (n=342) and log of weight-normalized blue-light stimulated luminescence field. We use the inverse-distance weighting (IDW) interpolation to generate a 10-cm-cell raster. This cell size exceeds the average spacing between portable OSL points (8 cm) and the average portable OSL sample width (~2-3 cm). We applied the IDW method using the Esri ArcMap Spatial Analyst toolbox, which renders the data in a smooth surface and includes geostatistical interpolation (e.g., contours rather than cell boundaries). In the IDW interpolation, we specified a power of 0.5 (Figure S5) to allow greater influence of each raster cell from adjacent points. This generates a smooth, rather than hummocky surface that is consistent with our interpretation of the sediment.

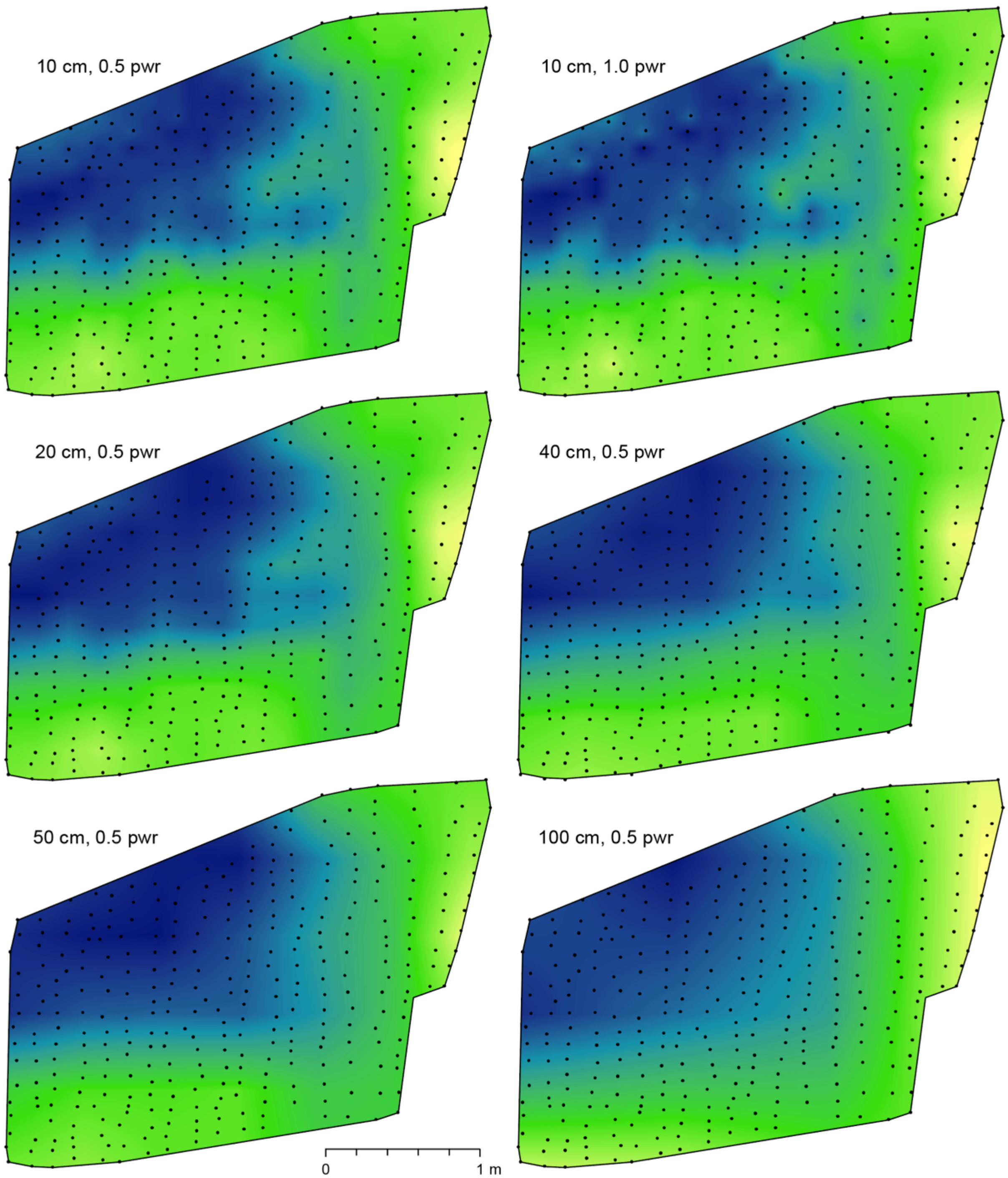

Figure S6. Inverse-distance weighting (IDW) interpolation of Deep Creek portable OSL data, showing raster surfaces varying from 10 to 100 cm cell sizes. Upper panel shows 10 cm raster surfaces calculated using a power (pwr) of 0.5 and 1.0.

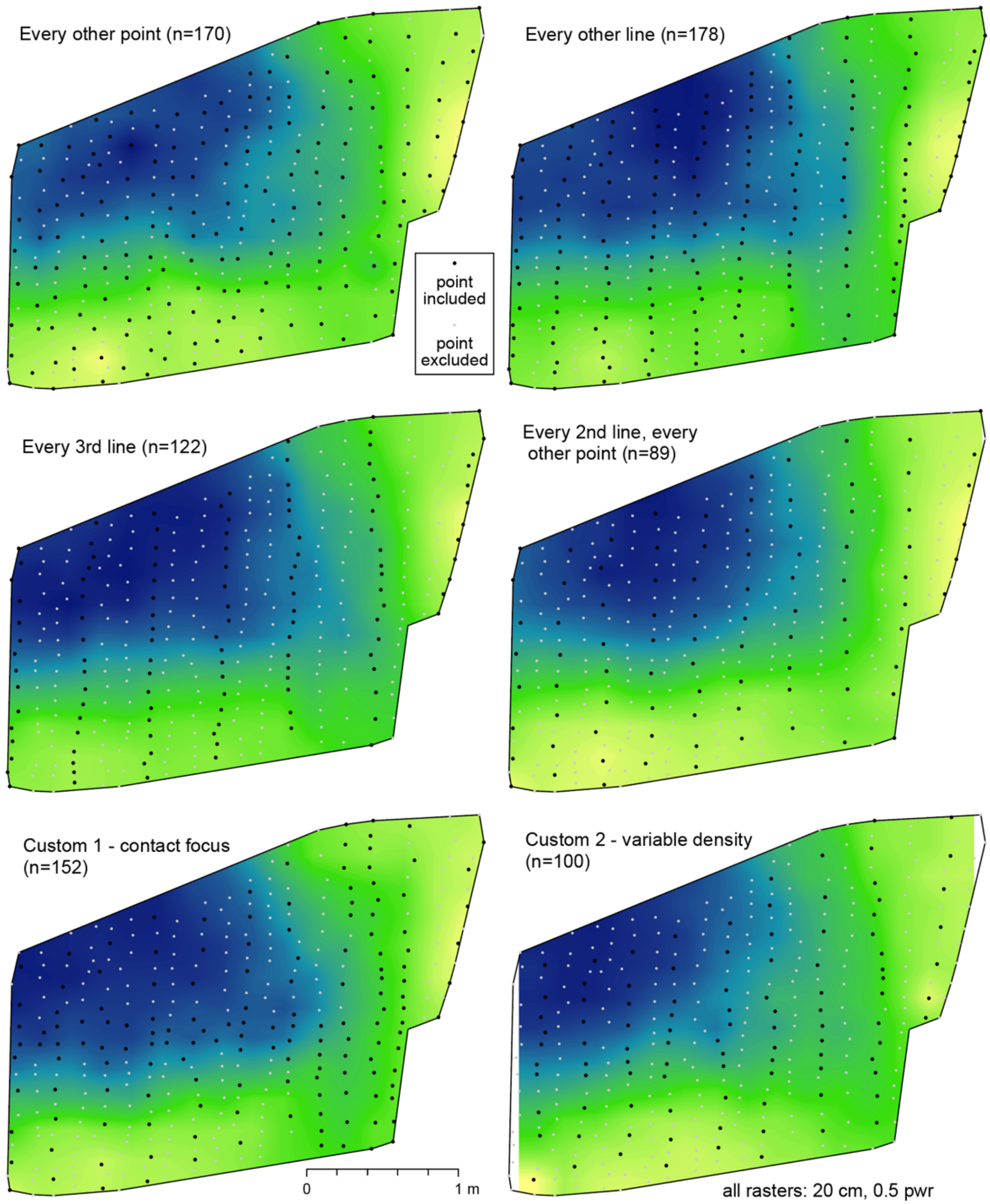

Figure S7. Inverse-distance weighting (IDW) interpolation of Deep Creek portable OSL data, with variable sample densities. Black points were included in the raster calculation; gray points were excluded. All surfaces generated using a 20 cm cell size and power (pwr) of 0.5.

We also generated raster surfaces using subsets of the portable OSL data (Figure S6). Subsets including about 50% of the original data (every other point, n=170 and every other line, n=178) reproduce the primary spatial relations observed in the full-density portable OSL raster. Subsets including ~30% of the original data as well as vertically oriented sample transects (every 3rd line, n=122 and custom 2, n=100) depict the expected spatial relations better than those with more distributed points (every 2nd line, every other point, n=89 and custom 1, n=152). This demonstrates that in a field application, lower density portable OSL sampling strategies in vertically oriented transects (across stratigraphic contacts) may be suitable for depicting first-order stratigraphic and pedogenic relations across an exposure.

OxCal Modeling

Supporting information includes OxCal Bayesian models constructed using ^{14}C and OSL ages presented above as well as previously published ^{14}C ages for the Deep Creek alluvial fan deposits and paleosol (Schwartz and Coppersmith, 1984; Jackson, 1991; Hylland and Machette, 2008). Models were constructed using OxCal version 4.4 (Bronk Ramsey, 2009).

Following DuRoss et al. (2018), we constructed three viable OxCal models for the Deep Creek site that include the majority of the available ^{14}C and OSL ages, but allow for the inclusion or exclusion of several ages (DC-R2, DC-R16, and DC-R22) that have a substantial impact on the resulting Deep Creek earthquake (DC1) time. These models result in DC1 earthquake times of ~0.4 ka, ~0.5 ka, and ~0.7 ka (Figures S8, S9, and S10, respectively). In Figure S11, two of these models are combined to generate a revised Deep Creek earthquake time (after DuRoss et al., 2018).

0.4-ka Deep Creek OxCal Model

OxCal Bayesian model for the Deep Creek site that includes ages DC-R2, DC-R16, and DC-R22 and results in a ~0.4-ka earthquake time (Figure S8).

```
Plot()
 {
 Sequence("0.4-ka Deep Creek OxCal Model")
  {
  Boundary("sequence start");
  Phase("alluvial fan")
   {
   C_Date("DC-L7", -11066, 544);
   R_Date("SC2-S&C1984", 7300, 1000);
   //Schwartz and Coppersmith (1984)
   C_Date("DC-L1", -5885, 462);
   C_Date("DC-L4", -5051, 423);
   C_Date("DC-L11", -4538, 283);
   R_Date("DC-R32", 4230, 20);
  };
  Phase("soil A horizon")
```

```
 {
  C_Date("DC-L2", -1679, 213);
  C_Date("DC-L5", -1120, 122);
  R_Date("DC-R15", 2890, 20);
  R_Date("DC-R4", 2820, 20);
  R_Date("DC-R9", 2370, 20);
  R_Date("DC-R21", 2310, 20);
  R_Date("DC-R1", 2030, 20);
  R_Date("DC-R10", 1880, 20);
  R_Date("DC-R5", 1600, 25);
  Delta_R("200±100 yr MRT", 200, 100);
  R_Date("L-DC-RC1-H&M08",1200, 80);
  //Hylland & Machette (2008)
  Delta_R("no MRT", 0, 0);
  R_Date("DC-R22", 730, 20);
  R_Date("DC-R2", 540, 20);
  R_Date("DC-R16", 355, 25);
  //R_Date("DC-R6", 130, 20);
  //R_Date("DC-R11", 0, 0);
 };
 Date("DC1");
 Phase("Colluvial wedge")
 {
  //R_Date("DC-R35", 4130, 35);
  //R_Date("DC-R18+R30", 3560, 55);
  //R_Date("DC-R26", 2500, 25);
  //R_Date("DC-R17", 2270, 40);
  //C_Date("DC-L9", 792, 125);
  //C_Date("DC-L8", -3579, 309);
  //R_Date("DC-R12+R13", 1310, 20);
  //C_Date("DC-L6", 922, 83);
  R_Date("DC-R27", 315, 55);
  C_Date("DC-L3", 1627, 35);
  R_Date("DC-R14", 280, 15);
  C_Date("DC-L10", 1726, 42);
  R_Date("DC-R8", 225, 15);
  R_Date("DC-R24b", 220, 15);
  R_Date("DC-R24a", 175, 20);
  //R_Date("DC-R7", 0, 0);
  //R_Date("DC-R19", 0, 0);
 };
 Boundary("historical record",1847 AD);
};
};
```

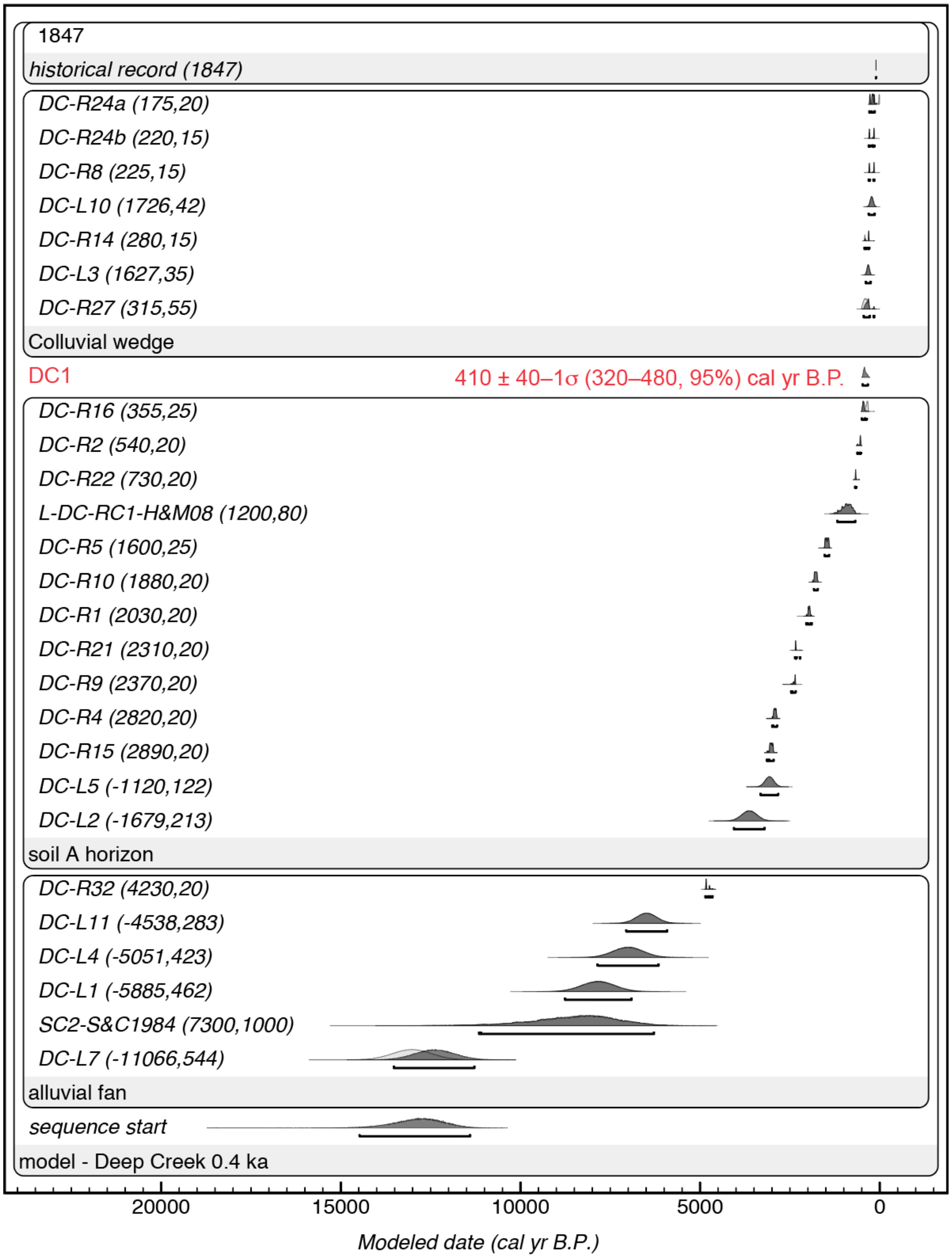

Figure S8. ^{14}C and OSL ages plotted in stratigraphic order and included in the 0.4-ka Deep Creek Bayesian model. Modeled ages constrain the time of Deep Creek earthquake DC1. Light- and dark-gray probability density function show prior and posterior distributions, respectively. Figure generated using OxCal version 4.4 (Bronk Ramsey, 2009).

0.5-ka Deep Creek OxCal Model

OxCal Bayesian model for the Deep Creek site that includes age DC-R22, excludes ages DC-R2 and DC-R16, and results in a ~0.5-ka earthquake time (Figure S9).

```
Plot()
 {
  Sequence("0.5-ka Deep Creek OxCal model")
  {
   Boundary("sequence start");
   Phase("alluvial fan")
   {
    C_Date("DC-L7", -11066, 544);
    R_Date("SC2-S&C1984", 7300, 1000);
    //Schwartz and Coppersmith (1984)
    C_Date("DC-L1", -5885, 462);
    C_Date("DC-L4", -5051, 423);
    C_Date("DC-L11", -4538, 283);
    R_Date("DC-R32", 4230, 20);
   };
   Phase("soil A horizon")
   {
    C_Date("DC-L2", -1679, 213);
    C_Date("DC-L5", -1120, 122);
    R_Date("DC-R15", 2890, 20);
    R_Date("DC-R4", 2820, 20);
    R_Date("DC-R9", 2370, 20);
    R_Date("DC-R21", 2310, 20);
    R_Date("DC-R1", 2030, 20);
    R_Date("DC-R10", 1880, 20);
    R_Date("DC-R5", 1600, 25);
    Delta_R("200±100 yr MRT", 200, 100);
    R_Date("L-DC-RC1-H&M08",1200, 80);
    //Hylland & Machette (2008)
    Delta_R("no MRT", 0, 0);
    R_Date("DC-R22", 730, 20);
    //R_Date("DC-R2", 540, 20);
    //R_Date("DC-R16", 355, 25);
    //R_Date("DC-R6", 130, 20);
    //R_Date("DC-R11", 0, 0);
   };
   Date("DC1");
   Phase("Colluvial wedge")
   {
    //R_Date("DC-R35", 4130, 35);
    //R_Date("DC-R18+R30", 3560, 55);
```

```
  //R_Date("DC-R26", 2500, 25);
  //R_Date("DC-R17", 2270, 40);
  //C_Date("DC-L9", 792, 125);
  //C_Date("DC-L8", -3579, 309);
  //R_Date("DC-R12+R13", 1310, 20);
  //C_Date("DC-L6", 922, 83);
  R_Date("DC-R27", 315, 55);
  C_Date("DC-L3", 1627, 35);
  R_Date("DC-R14", 280, 15);
  C_Date("DC-L10", 1726, 42);
  R_Date("DC-R8", 225, 15);
  R_Date("DC-R24b", 220, 15);
  R_Date("DC-R24a", 175, 20);
  //R_Date("DC-R7", 0, 0);
  //R_Date("DC-R19", 0, 0);
 };
 Boundary("historical record",1847 AD);
 };
};
```

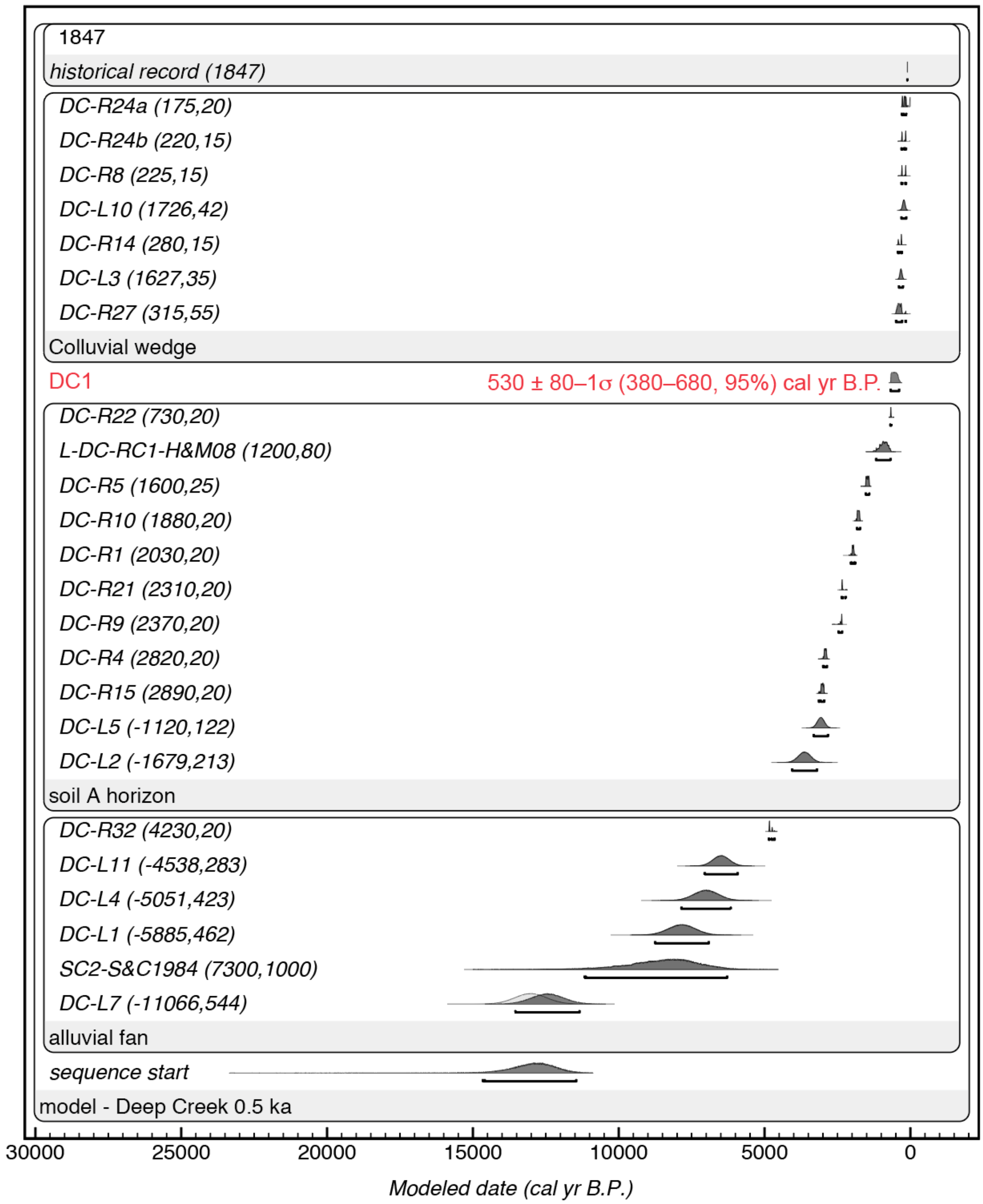

Figure S9. ^{14}C and OSL ages plotted in stratigraphic order and included in the 0.5-ka Deep Creek Bayesian model. Modeled ages constrain the time of Deep Creek earthquake DC1. Light- and dark-gray probability density function show prior and posterior distributions, respectively. Figure generated using OxCal version 4.4 (Bronk Ramsey, 2009).

0.7-ka Deep Creek OxCal Model

OxCal Bayesian model for the Deep Creek site that excludes ages DC-R22, DC-R2, and DC-R16, and results in a ~0.7-ka earthquake time (Figure S10).

```
Plot()
 {
  Sequence("0.7-ka Deep Creek OxCal Model")
  {
   Boundary("sequence start");
   Phase("alluvial fan")
   {
    C_Date("DC-L7", -11066, 544);
    R_Date("SC2-S&C1984", 7300, 1000);
    //Schwartz and Coppersmith (1984)
    C_Date("DC-L1", -5885, 462);
    C_Date("DC-L4", -5051, 423);
    C_Date("DC-L11", -4538, 283);
    R_Date("DC-R32", 4230, 20);
   };
   Phase("soil A horizon")
   {
    C_Date("DC-L2", -1679, 213);
    C_Date("DC-L5", -1120, 122);
    R_Date("DC-R15", 2890, 20);
    R_Date("DC-R4", 2820, 20);
    R_Date("DC-R9", 2370, 20);
    R_Date("DC-R21", 2310, 20);
    R_Date("DC-R1", 2030, 20);
    R_Date("DC-R10", 1880, 20);
    R_Date("DC-R5", 1600, 25);
    Delta_R("200±100 yr MRT", 200, 100);
    R_Date("L-DC-RC1-H&M08",1200, 80);
    //Hylland & Machette (2008)
    Delta_R("no MRT", 0, 0);
    //R_Date("DC-R22", 730, 20);
    //R_Date("DC-R2", 540, 20);
    //R_Date("DC-R16", 355, 25);
    //R_Date("DC-R6", 130, 20);
    //R_Date("DC-R11", 0, 0);
   };
   Date("DC1");
   Phase("Colluvial wedge")
   {
    //R_Date("DC-R35", 4130, 35);
    //R_Date("DC-R18+R30", 3560, 55);
```

```
  //R_Date("DC-R26", 2500, 25);
  //R_Date("DC-R17", 2270, 40);
  //C_Date("DC-L9", 792, 125);
  //C_Date("DC-L8", -3579, 309);
  //R_Date("DC-R12+R13", 1310, 20);
  //C_Date("DC-L6", 922, 83);
  R_Date("DC-R27", 315, 55);
  C_Date("DC-L3", 1627, 35);
  R_Date("DC-R14", 280, 15);
  C_Date("DC-L10", 1726, 42);
  R_Date("DC-R8", 225, 15);
  R_Date("DC-R24b", 220, 15);
  R_Date("DC-R24a", 175, 20);
  //R_Date("DC-R7", 0, 0);
  //R_Date("DC-R19", 0, 0);
 };
 Boundary("historical record",1847 AD);
 };
};
```

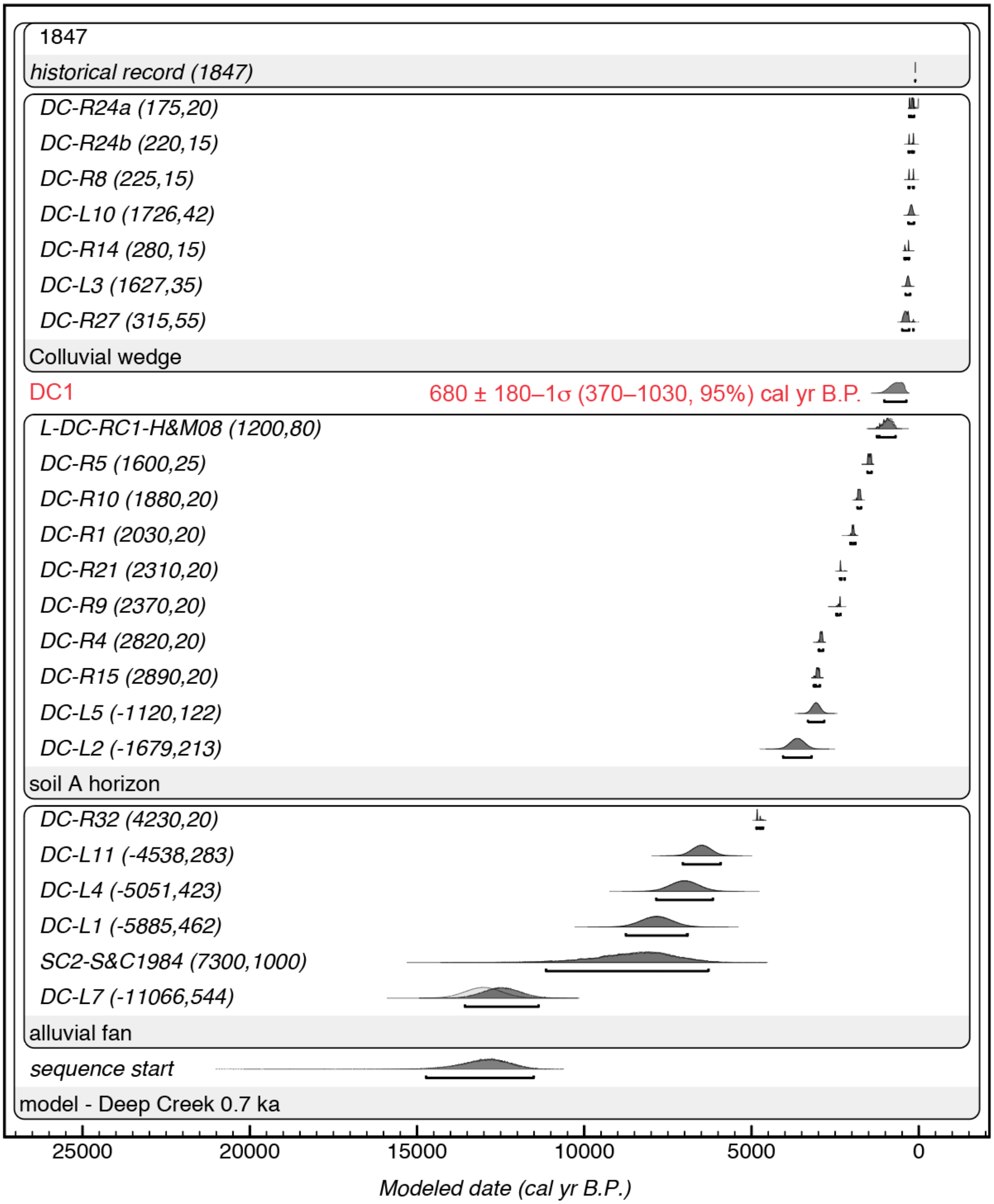

Figure S10. [14]C and OSL ages plotted in stratigraphic order and included in the 0.7-ka Deep Creek Bayesian model. Modeled ages constrain the time of Deep Creek earthquake DC1. Light- and dark-gray probability density function show prior and posterior distributions, respectively. Figure generated using OxCal version 4.4 (Bronk Ramsey, 2009).

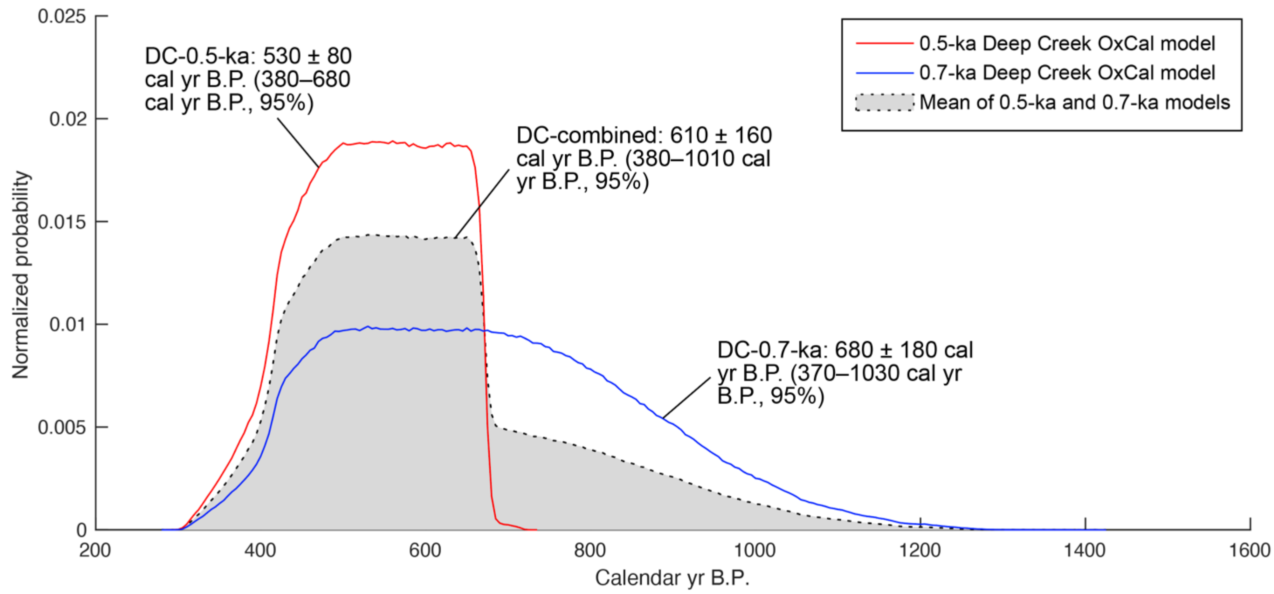

Figure S11. Revised Deep Creek earthquake time (gray-shaded earthquake-timing probability density function [PDF]) based on the bin-wise mean of earthquake PDFs generated in the 0.5-ka (red) and 0.7-ka (blue) OxCal Bayesian models.

REFERENCES

Bronk Ramsey, C., 2009, Bayesian analysis of radiocarbon dates: Radiocarbon, v. 51, p. 337–360, doi:10.1017/S0033822200033865.

DuRoss, C.B., Bennett, S.E.K., Briggs, R.W., Personius, S.F., Gold, R.D., Reitman, N.G., Hiscock, A.I., and Mahan, S.A., 2018, Combining conflicting Bayesian models to develop paleoseismic records: An example from the Wasatch fault zone, Utah: Bulletin of the Seismological Society of America, v. 108, p. 3180–3201, doi:10.1785/0120170302.

Galbraith, R.F., and Roberts, R.G., 2012, Statistical aspects of equivalent dose and error calculation and display in OSL dating: An overview and some recommendations: Quaternary Geochronology, v. 11, p. 1–27, doi:10.1016/j.quageo.2012.04.020.

Gray, H.J., DuRoss, C.B., Gold, R.D., and Nicovich, S.R., 2021, Geochronological data for the Deep Creek paleoseismic site, Wasatch fault zone, Utah: U.S. Geological Survey data release, doi:doi:10.5066/P9YX88LK.

Gray, H.J., Mahan, S.A., Rittenour, T., and Nelson, M.S., 2015, Guide to luminescence dating techniques and their application for paleoseismic research, *in* Proceedings volume, Basin and Range Province Seismic Hazards Summit III (BRPSHSIII), Utah Geological Survey Miscellaneous Publication 15–5, https://ugspub.nr.utah.gov/publications/misc_pubs/mp-15-5/mp-15-5_invited_paper.pdf.

Gray, H.J., Mahan, S.A., Springer, K.B., and Pigati, J.S., 2018, Examining the relationship between portable luminescence reader measurements and depositional ages of paleowetland sediments, Las Vegas Valley, Nevada: Quaternary Geochronology, v. 48, p. 80–90, doi:10.1016/j.quageo.2018.07.006.

Hylland, M.D., and Machette, M.N., 2008, Surficial geologic map of the Levan and Fayette segments of the Wasatch fault zone, Juab and Sanpete counties, Utah: Utah Geological Survey Map 229.

Jackson, M., 1991, The number and timing of Holocene paleoseismic events on the Nephi and Levan segments, Wasatch fault zone, Utah: Utah Geological Survey Special Study 78, v. Paleoseismology of Utah, Volume 3, p. 1–23.

Kreutzer, S., Schmidt, C., Fuchs, M.C., Dietze, M., Fischer, M., and Fuchs, M., 2012, Introducing an R package for luminescence dating analysis: Ancient TL, v. 30, p. 1–8.

Reimer, P.J. et al., 2020, The IntCal20 Northern Hemisphere Radiocarbon Age Calibration Curve (0–55 cal kBP): Radiocarbon, v. 62, p. 725–757, doi:10.1017/RDC.2020.41.

Reitman, N.G., Bennett, S.E.K., Gold, R.D., Briggs, R.W., and DuRoss, C.B., 2015, High-resolution trench photomosaics from image-based modeling: Workflow and error analysis: Bulletin of the Seismological Society of America, v. 105, p. 2354–2366, doi:10.1785/0120150041.

Sanderson, D.C.W., and Murphy, S., 2010, Using simple portable OSL measurements and laboratory characterisation to help understand complex and heterogeneous sediment sequences for luminescence dating: Quaternary Geochronology, v. 5, p. 299–305, doi:10.1016/j.quageo.2009.02.001.

Schwartz, D.P., and Coppersmith, K.J., 1984, Fault behavior and characteristic earthquakes: Examples from the Wasatch and San Andreas Fault Zones: Journal of Geophysical Research: Solid Earth, v. 89, p. 5681–5698, doi:10.1029/JB089iB07p05681.

Stone, A., Bateman, M.D., Burrough, S.L., Garzanti, E., Limonta, M., Radeff, G., and Telfer, M.W., 2019, Using a portable luminescence reader for rapid age assessment of aeolian sediments for reconstructing dunefield landscape evolution in southern Africa: Quaternary Geochronology, v. 49, p. 57–64, doi:10.1016/j.quageo.2018.03.002.

Stone, A.E.C., Bateman, M.D., and Thomas, D.S.G., 2015, Rapid age assessment in the Namib Sand Sea using a portable luminescence reader: Quaternary Geochronology, v. 30, p. 134–140, doi:10.1016/j.quageo.2015.02.002.